Hindawi Publishing Corporation
Journal of Nanomaterials
Volume 2010, Article ID 396214, 11 pages
doi:10.1155/2010/396214

Research Article

Measurement and Optimization of Metal-Nanoparticle-Induced Luminescence Enhancement Factors in a Crossed-Optical Fiber Configuration

Maria Veronica Rigo and Peter Geissinger

Department of Chemistry & Biochemistry, University of Wisconsin-Milwaukee, 3210 N. Cramer Street, Milwaukee, WI 53211-3029, USA

Correspondence should be addressed to Peter Geissinger, geissing@uwm.edu

Received 14 September 2010; Accepted 7 November 2010

Academic Editor: Kui Yu

A crossed-optical-fiber configuration comprised of silver nanoparticles covalently attached to the core of an optical fiber and labeled with luminescent ruthenium molecules is reported. A second optical fiber was placed at right angle of the fiber containing the nanoparticle/ruthenium, to form a fiber-fiber junction, and it was used to detect the luminescence from the ruthenium molecules bound to the first fiber. To employ the effect of metal-enhanced luminescence, the ruthenium complex was kept at an appropriate distance from the nanoparticles by polyelectrolyte spacer layers. For silver nanospheres, nanotriangles and nanorods and for spacer-layer thicknesses from 2–14 nm luminescence-enhancement factors were determined. A 27-fold luminescence enhancement was found when the ruthenium complex was placed 4 nm from silver nanotriangles. Finally, a calibration curve for the oxygen dependence of luminescence intensities and lifetimes of ruthenium complex is presented suggesting that the oxygen sensing capabilities of the nanoengineered-ruthenium complex are maintained.

1. Introduction

Metal nanoparticles and nanostructured metal films possess localized surface plasmon resonances (LSPRs) that confer upon these materials a number of unique and useful optical properties. These plasma oscillations are resonant in the optical regime at frequencies that can be tuned by engineering the nanoparticle size and shape and surrounding media [1–5]. Furthermore, plasmons strongly influence the optical properties of luminophores that are located at a short distance from metal nanoparticles (Nps) according to different mechanisms. First, an increase of the luminophore excitation rate occurs as a consequence of the metallic Np local-field enhancement via localized plasmon excitation. The maximum excitation-rate enhancement occurs when the luminophore absorption band coincides with the metal Np plasmon resonance wavelength [6]. The second mechanism involves the modification of the luminophore radiative decay rate (RDR) with a concomitant increase in its luminescence quantum yield and a decrease of its luminescence lifetime. The RDR can be enhanced when the emission band of the luminophore coincides with the LSPR of the Nps [7]. Furthermore, a simultaneous reduction of both lifetime and quantum efficiency of a luminophore may occur as a result of luminescence quenching by the metal. This arises when a luminophore is in close proximity of the metal surface; then, electromagnetic coupling of the luminophore to the plasma resonance provides a damping channel. In the case of a luminophore with high quantum efficiency, the metal-mediated RDR remains almost unchanged and the quenching effect predominates if the luminophore is too close to the metal surface [8].

During the last decade, experiments have led to the observation of photoluminescence enhancement and quench-

ing, depending on the distance between luminophore and metal [9], with associated changes in excited state lifetime [10, 11]. In addition to this distance dependence, the local-field enhancements in proximity of metal nanostructures are strongly wavelength dependent, and it is expected that the amount of luminescence enhancement or quenching will also depend on the spectral overlap between the luminophore and the LSPR modes of the nanoparticle [4, 12].

In this paper the modification of the radiative decay rate of the luminophore bis (2,2′-bipyridine)-(5-isothiocyanatophenanthroline) ruthenium through the metal-enhanced-luminescence (MEL) phenomenon is demonstrated in a crossed-fiber sensor array configuration developed in our laboratory [13–15]. First we demonstrated the importance of the coupling between the silver nanoparticles plasmon modes and the emission band of ruthenium complex for modifying its RDR. Next we studied the distance and wavelength dependence of the MEL phenomena in the fiber-fiber system. Finally we tested the response of the enhanced luminophore towards gaseous oxygen for potential real-time and remote oxygen monitoring.

2. Experimental

2.1. Reagents and Materials. Silver nitrate, sodium citrate, sodium borohydrate, poly(vinyl pyrrolidone) with a molecular weight of ~55000, cetyltrimethylammonium bromide (CTAB), (3-aminopropyl)trimethoxysilane (APS), (2, 2′-bipyridine)-(5-isothiocyanato-phenanthroline) ruthe-nium (RuBITC), hydrogen peroxide solution (30 wt.% in water), poly(allylamine hydrochloride) (PAH) with molecular weight of 50000, poly(styrene sulfonate) (PSS) with molecular weight of 70000, sodium chloride, potassium hydroxide (KOH), and potassium cyanide (KCN) were obtained from Sigma Aldrich Chemical Company (Milwaukee, WI). Rhodamine B isothiocyanate (RBITC) was purchased from VWR International.

All setups and experiments used multimode silica fibers with a TECS (trademark of 3M Corp.) cladding (FT-200-UMT with core diameter of 200 μm) and SMA 905 connectors purchased from ThorLabs, Inc. (Newton, NJ). The fibers had core and cladding refractive indices of n_{co} = 1.457 and n_{cl} = 1.404, respectively. Deionized water (DI) with a resistivity of 18 MΩ·cm was used for all aqueous experiments. All reagents were used as received without further purification.

2.2. Preparation of Silver Nanoparticles. Silver nanospheres (AgNS) are synthesized from reducing silver salt with citrate which can provide various sizes of silver nanoparticles with a relatively reasonable size distribution (in this work the AgNS size is 30 ± 2.1 nm with a yield of 95% of spherical particles) [16]. Size measurement was performed using the available software ImageJ (http://rsbweb.nih.gov/ij/index.html). For each sample analysis, 4 representative TEM images (not shown here) were selected and the individual particles were counted. Histograms and Gaussian fits were then obtained for size distribution analysis. Silver nanorods (AgNR) are prepared by a seeding growth approach in the presence of an aqueous CTAB micelle template [17] giving nanorods (nanorod yield ~70%; remainder consisting of spherical nanoparticles), with respect ratios of 3 ± 0.5 (30 ± 1.62 nm/10 ± 3 nm: long/short axis) and 12 ± 3.9 (120 ± 4.34 nm/10 ± 1.11 nm: long/short axis). Silver nanotriangles (AgNT, yield ~80% among polymorphological shapes) with a base length of 89 ± 3.2 nm were obtained by the method reported by Deivaraj et al. [18].

To attach AgNps and/or molecules to the fiber core, the original fibers were modified by first removing the fibers jackets by mechanical stripping. Subsequently, the cladding layers were removed by heating followed by rubbing with a cotton swab immersed in acetone. The exposed core was further cleaned using Piranha solution (3 : 1 concentrated sulfuric acid: 30% hydrogen peroxide solution) to eliminate organic residue and hydroxylate the silica surface. Using this method two regions where created in two different optical fibers, then the fibers where positioned orthogonal to each other to form the fiber-fiber junctions. Only one of the fibers was used to attach the nanoparticles and the molecules to be tested (referred to as excitation fiber). The second fiber was used only as a detection system (referred to as detection fiber).

2.3. Preparation of Intensity Reference Region. The first fiber region (on the excitation fiber) is used as an intensity reference, that is to monitor and to correct for fluctuations of the laser light source. The nonmetalized reference region of the fiber array was first treated with a solution of 60% water, 39% methanol, and 1% 8 mM KOH for 1 h to create a negative charge on the fiber-core surface. Then the region was washed with DI water and dried under flowing nitrogen. The negatively charged surface region was dipped in a PAH~RBITC solution and left for 2 hours at room temperature and subsequently washed with DI water three times and dried with nitrogen gas. To covalently attach RBITC to PAH, first 100 mg of PAH was dissolved in 10 ml DI water; then a 3-M KOH solution was added dropwise, while stirring to adjust the pH of the PAH solution to 9.4. Next, 2 mg of RBITC was added, and the solution was stirred in darkness overnight. To remove the unreacted RBITC, the reaction mixture was dialyzed (Spectra 8-kDa cutoff) against ultrapure water; the purified product is now referred to as PAH~RBITC. Only a small fraction of the available amino groups was labeled; thus, the net charge remained positive, which facilitated further adsorption by the negatively charged polyelectrolyte.

2.4. Preparation of Metalized Region. The second region on the excitation fiber was used to attach AgNps. Thus, the silica surface of the fiber core was treated with 1% ethanolic solution of APS for 2 hours (see Figure 1). The excess and nonadhesive APS layer was rinsed three times with DI water and ethanol. Next, the activated-core was coated with a highly concentrated solution of AgNps for 12 hours at room temperature (for all the shapes, AgNps solutions with absorbance of ~4 were used), afterwards the functionalized

core was washed with DI water and dried with nitrogen gas. To study the distance dependence of the metal-enhanced RuBITC-luminescence we employed the well-known Layer-by-Layer (LbL) deposition [19, 20] of oppositely charged polyelectrolytes onto a AgNp-coated optical fiber to create spacer layers with a well-defined thickness. In a typical LbL deposition, stock solutions of PSS and PAH (100 mg in 10 mL of DI water, pH ~ 6.5) were prepared and sonicated for 20 min. The ionic strength of the polyelectrolyte solutions was adjusted with 0.1 M sodium chloride. In the first stage, the negatively charged AgNps (covalently bound to the fiber core) were immersed in PAH solution for 2 hours at room temperature and subsequently washed with DI water three times. Then the functionalized core was dried in a stream of nitrogen gas. The positively charged fiber~AgNp-PAH assembly was used for the next polyelectrolyte deposition with PSS, following the same procedure as described for the deposition of PAH. LbL assembly of PAH-PSS on AgNp-functionalized fiber cores was carried out manually and repeated to build spacer layers with increasing thickness. The last step in the LbL assembly was to functionalize the outermost polyelectrolyte layer with PAH~RuBITC. PAH~RuBITC was synthesized using the same protocol used for PAH~RBITC (reference luminophore) because RuBITC contains an isothiocyanate group able to react with the amino moiety of PAH.

2.5. Instrumentation. To investigate the wavelength dependence of the plasmon-mediated local field enhancement, a pulsed dye laser (PTI PL201) pumped by a nitrogen laser (PTI PL2300 with pulse width 0.6 ns, pulse energy 1.4 mJ, pulse repetition rates of 3–10 Hz) was used as the excitation source for the system (wavelength range 410 nm to 465 nm). The experimental setup is illustrated in Figure 2. A pair of lenses was employed to couple the laser light into the excitation fiber (which is the one that was chemically modified). The first region in the fiber array contained the intensity reference molecule, rhodamine B isothiocyanate, whereas in the second region ruthenium, the oxygen sensor molecule, was located. The luminescence emitted by the regions was captured by optical fibers (detection fibers, see Figure 2) crossing at right angle to the fiber carrying the excitation light pulse and guided to the detector. The RuBITC luminescence pulse was delayed by passage through an additional stretch of fiber (10 m) to arrive at a photomultiplier tube (PMT1 Burle C31034A; with Peltier cooling) after the reference signal had subsided. A narrow bandpass filter (NBPF) (610 nm, Edmunds J43-079) was used in front of the PMT1 (set at 1.6 kV) to select the RuBITC and RBITC pulses. The output current of PMT1, which was analyzed with a LeCroy LC564DL digital storage oscilloscope (DSO, bandwidth 1 GHz, sampling rate 4 GS/s), displayed both sensor signals sequentially in one trace. A trigger for the DSO was generated using a second photomultiplier tube (PMT2—RCA 1P28, 1.6-ns rise time), which collected light scattered off the front face of the excitation fiber. The fiber-fiber junctions were mounted in a home-built flow cell, which could be filled with mixtures of oxygen and nitrogen gases from pure gas cylinders (Praxair grade 2.6 and 4.8, resp.) at different partial pressures. No photobleaching or photodecomposition of RuBITC or/and RBITC were observed. All measurements for the calculation of enhancement factors and lifetime ratios, in which spacer-layer thickness and excitation wavelength were varied, were carried out in a nitrogen atmosphere.

Absorption spectra were recorded using a Perkin Elmer Lambda 650 spectrometer, while the emission spectrum of the luminophore was obtained using a SPEX 1681, 0.22 m Fluorolog spectrometer.

2.6. Data Treatment. A typical set of emission pulses obtained from two crossed-fiber regions is shown in Figure 3(a) (3000 pulse traces were averaged); the first peak results from the emission of PAH~RBITC, whereas the second one, delayed with respect to the first one and fully resolved in time, is the RuBITC decay curve (PAH~RuBITC). Using OriginPro 7 software (OriginLab) the areas of both peaks were calculated (I) and the referenced RuBITC intensity ($\widetilde{I}$) was calculated according to

$$\widetilde{I} = \frac{I_{\text{RuBITC}}}{I_{\text{RBITC}}}. \tag{1}$$

To be consistent from one set of time traces to another, we calculated the peak areas over the same time intervals, and baseline correction was also applied to the data.

Luminescence lifetimes were determined from the averaged RuBITC (PAH~RuBITC) pulse shapes by fitting the trailing part of the RuBITC luminescence pulse. No deconvolution of the signal pulses with the shape of the excitation light pulse had to be carried out because the excitation-light pulse at the sensor region is three orders of magnitude smaller than the RuBITC luminescence lifetime. The luminescence-intensity decays of ruthenium were analyzed in terms of a multiexponential model [21] as the sum of individual single-exponential decays:

$$I(t) = \sum_{i=1}^{n} \alpha_i \exp\left(\frac{-t}{\tau_i}\right). \tag{2}$$

In this expression, τ_i represents the decay times of the excited state, α_i represents the pre-exponential weighting factors, and $\sum \alpha_i = 1.0$. The fractional contribution of each component to the steady state intensity is described by

$$f_i = \frac{\alpha_i \tau_i}{\sum \alpha_i \tau_i}, \tag{3}$$

where f_i is the fractional contribution of the single decay i to the total time traces. The α_i's and τ_i's can be extracted from the decays curve by fitting them with (2), assuming that the decay pulse is a sum of exponentials. These were determined using OriginPro 7 graphic software from the least-squares fitting process (bi-exponential fit). The goodness of fit was determined by the R value. Then the average lifetime ($\overline{\tau}$) is represented by

$$\overline{\tau} = \sum f_i \tau_i. \tag{4}$$

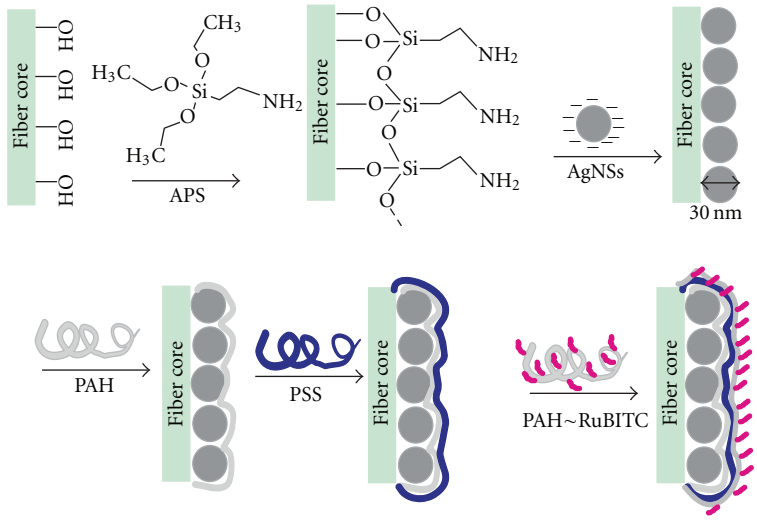

Figure 1: Schematic representation of the LbL assembly on the sensor region of the excitation fiber: (a) the surface of the fiber core is initially functionalized with amines (APS) to render a chemical surface for AgNS (•) attachment, (b) the thickness of the spacer layer is increased by adsorption of a polycation (PAH in grey) and a polyanion (PSS in dark blue), (c) once the desired thickness is accomplished the luminescent PAH~RuBITC layer (in magenta) was deposited. Each layer (PAH/PSS) has a thickness of ~2 nm. The same procedure was used for different AgNp shapes.

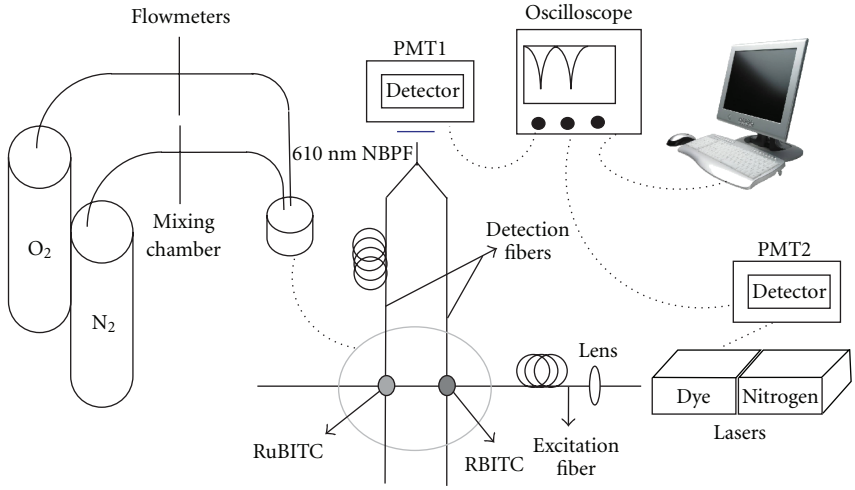

Figure 2: Experimental setup of the sensor system.

3. Results and Discussion

3.1. Quantification of the Enhancement of RuBITC Luminescence. The plasmonic effect of the metal nanoparticles (Nps) on the luminescence of RuBITC can be quantified by evaluating the ratio of the referenced-luminescence intensity, $\widetilde{I}$, (or of the luminescence lifetime $\overline{\tau}$) in presence and absence of metal Nps. Therefore, the luminescence-intensity enhancement factor η and the luminescence lifetime ratio $\widetilde{\tau}$ were written as

$$\eta = \frac{\widetilde{I}_{\text{Metal}}}{\widetilde{I}_{\text{NonMetal}}}, \qquad \widetilde{\tau} = \frac{\overline{\tau}_{\text{Metal}}}{\overline{\tau}_{\text{NonMetal}}}, \tag{5}$$

where $\widetilde{I}_{\text{Metal}}$ and $\overline{\tau}_{\text{Metal}}$ are the referenced ruthenium luminescence intensity and lifetime, respectively, in the presence of the metal Nps. $\widetilde{I}_{\text{NonMetal}}$ and $\overline{\tau}_{\text{NonMetal}}$ are the respective referenced intensity and lifetime of ruthenium without metal Nps. For a precise comparison of the photophysical behavior of RuBITC in the presence and absence of AgNps, potassium cyanide (KCN, 0.1 mM) was added to the metalized nanosystem to dissolve the metal Nps. Dissolution of the AgNps created voids which retained the shape of the Np that formerly occupied this space. In fact, the structure of the entire sensor assembly remained unchanged when the AgNps were removed [20]. Thus, a comparison of the luminescence properties of the sensor assembly with AgNps and after removal of the AgNps allows for the quantitative determination of η and $\widetilde{\tau}$, using identical RuBITC concentrations and

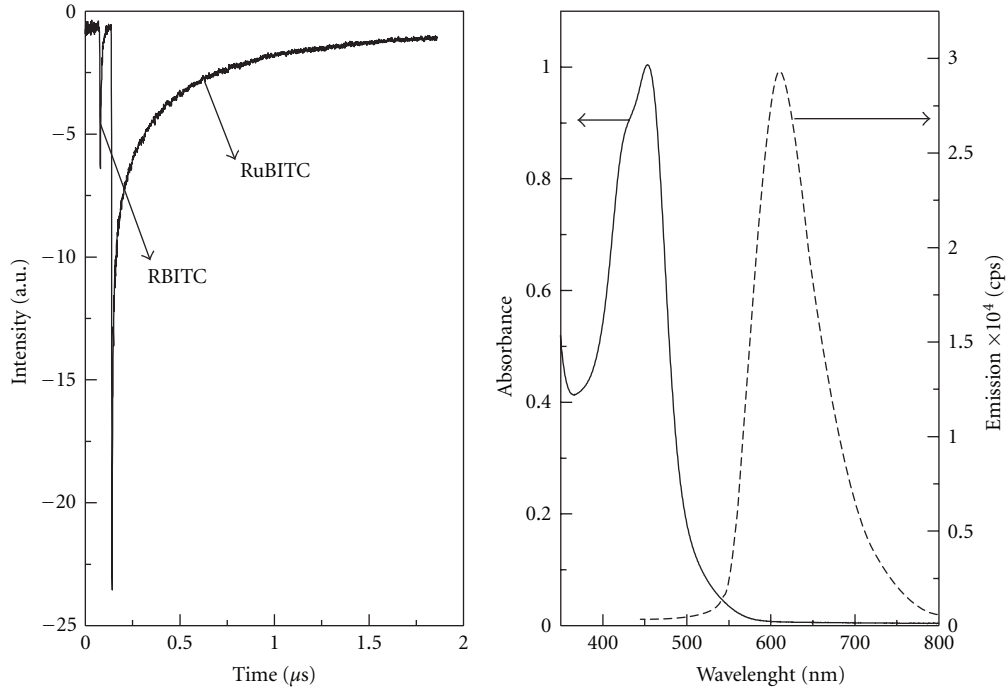

FIGURE 3: (a) Raw data corresponding to the output of two sensor regions resolved in time. The first pulse corresponds to the reference dye, RBITC, and the second one consists of the RuBITC decay curve. (b) Absorption and emission spectra of a 3-mM RuBITC solution.

identical system structure (i.e., same spacer-layer thicknesses and distances to the fiber core). Therefore, η and $\widetilde{\tau}$ before and after removal of the AgNps reflect only the effect of AgNps on the optical properties of RuBITC.

Coating the core of the excitation fiber with a structure consisting of AgNps, dielectric spacer layers, and ruthenium ((Fiber core-AgNps–$(PAH\text{-}PSS)_n$-PAH~RuBITC); n = number of individual polyelectrolyte (double) spacer layers), we were able to evanescently excite the AgNp plasmon modes as well as the ruthenium molecules, and capture, through the detection fiber, nanosystem. Once we measured $\widetilde{I}_{\text{Metal}}$ and $\overline{\tau}_{\text{Metal}}$ the AgNps were removed to calculate the η and $\widetilde{\tau}$ factors (5).

For each configuration of a sensor region (i.e., for a given nanoparticle shape and a specific spacer-layer thickness) the results of three different experiments were averaged (using each time a newly synthesized sensor-region assembly). In each experiment 3000 luminescence pulse traces were averaged and the error bars were calculated using Student's t-value for the 95% confidence level ($n = 3$). Prior to these measurements, we recorded control emission spectra to test for the possibility of light being scattered by AgNps and coupled across the fiber junction at the sensor region. These control spectra were important because one can obtain large scattering intensities from the metal particles, which are known to be strong scattering centers [22]. This could affect the calculation of η and $\widetilde{\tau}$. For these measurements, fiber junctions were prepared that were identical in structure to the RBITC reference and the RuBITC probe region, expect that the RuBITC was omitted in its region and only the AgNps and spacer layers were present. We found that the 610-nm narrow bandpass filter placed in front of PMT1 effectively removed any light scattered by the AgNps deposited at the fiber junction; thus, only the luminescence of RuBITC was detectable by PMT1 in that region.

The equations provided by Lakowicz et al. [7] for the luminescence quantum yield and the luminescence lifetime of a luminescent dye interacting with metal surfaces allow for estimating the quantum yield Q_{Metal} of the ruthenium dye in the presence of nanoparticles. From Lakowicz' equations, we derived

$$Q_{\text{Metal}} = \widetilde{\tau}(Q_{\text{NonMetal}} - 1) + 1, \tag{6}$$

where Q_{NonMetal} is the luminescence quantum yield of the ruthenium dye in the absence of metal nanoparticles. Using the method described in [23], we measured the quantum yield of this dye in ethanol solution using rhodamine 101 as a standard. Using this value to approximate the luminescence quantum yield of the ruthenium dye in the absence of metal nanoparticles, Q_{Metal} can be estimated from the measured lifetime ratios $\widetilde{\tau}$. In spite of this approximation, the estimated quantum yields provide some guidance on the extent of RDR modification when maximum enhancement is observed.

3.2. Nanoparticle Shape Dependence of the RuBITC Luminescence Enhancement. First, the effect of spectral overlap between the ruthenium absorption band and the plasmon bands of AgNSs, AgNTs, and AgNRs was analyzed using a fixed excitation wavelength of 465 nm, which is optimal for

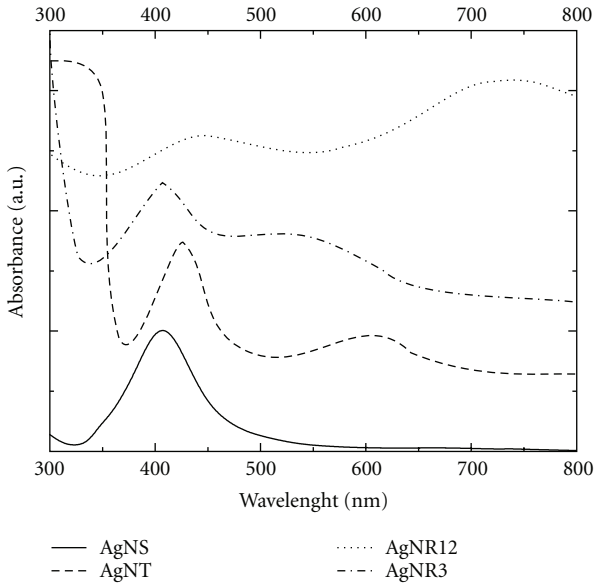

Figure 4: Plasmonic modes of AgNps colloidal solutions: (-) silver nanospheres, (- -) silver nanotriangles, (– · –) silver nanorods with aspect ratio of 3, and (· · · · ·) silver nanorods with aspect ratio of 12.

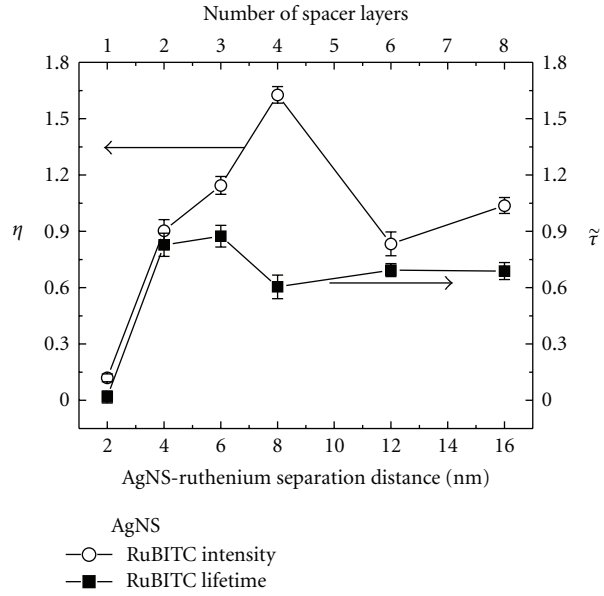

Figure 5: Enhancement factors η and lifetime ratios $\tilde{\tau}$ as function of the total spacer layer thickness d (bottom axis) and number n of polyelectrolyte (double) layers (top axis) for the fibercore~AgNS-$(PAH\text{-}PSS)_n$-$(PAH\sim RuBITC\text{-}PSS)_4$ assemblies.

ruthenium excitation as seen in Figure 3(b). For AgNSs, the maximum of the plasmon absorption band is located at ~410 nm (see Figure 4); it is attributed to the plasmon dipole resonance of the spherical metal nanoparticles. To investigate the modification of the ruthenium radiative decay rate (RDR) by the AgNS (diameter ~30 nm), the ruthenium complex was placed at different distances from the AgNSs by varying the number of polyelectrolyte layers. Each individual polyelectrolyte (double) layer (PAH-PSS) had a thickness of ~2 nm as calculated from TEM images. Using just one ruthenium-doped layer (PAH~RuBITC-PSS), which was electrostatically attached to the outermost nonfunctionalized layer, we were not able to detect any luminescence from the complex when excited at 465 nm. To overcome this problem we deposited three additional (PAH~RuBITC-PSS)-functionalized shells to obtain measurable luminescence. For all the experiments we defined thickness d (henceforth referred to as "spacer-layer thickness") as the total distance from the nanoparticle surface to the first RuBITC-functionalized polyelectrolyte layer, excluding the functionalized layer(s).

The measured values of η and $\tilde{\tau}$ for the AgNS-$(PAH\text{-}PSS)_n$-$(PAH\sim RuBITC\text{-}PSS)_4$ assemblies are shown in Figure 5 and summarized in Table 1. It can be seen that when the ruthenium-doped layer was separated by $d \sim 2$ nm from the metal nanoparticles, the dissipation of energy by the nonradiative pathway is the predominant mechanism because both luminescence intensity and lifetime were quenched. When ruthenium-doped layer was placed at a distance of ~4 nm from the AgNps, the overall quenching was reduced. With a spacer-layer thickness of 8 nm, the ruthenium emission intensity increased whereas the lifetime decreased, suggesting a modification of the RDR. When the spacer-layer thickness

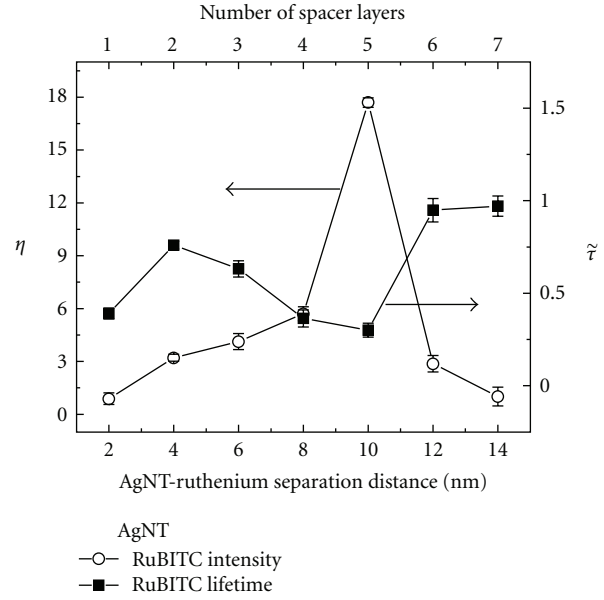

Figure 6: Enhancement factors η and lifetime ratios $\tilde{\tau}$ as function of the total spacer layer thickness d (bottom axis) and number n of polyelectrolyte (double) layers (top axis) for the fibercore~AgNT-$(PAH\text{-}PSS)_n$-$(PAH\sim RuBITC\text{-}PSS)_4$ assemblies.

was further increased, ruthenium apparently no longer experienced the plasmon-based metal effect and both intensity and lifetime of RuBITC assumed values close to those of the nonmetalized system. A maximum luminescence-enhancement factor of $\eta \sim 1.6$ and a minimum lifetime ratio of $\tilde{\tau} \sim 0.60$ were found when the first ruthenium-doped layer was separated by ~8 nm from the AgNS. Because of

the good spectral overlap of the ruthenium absorption band with the AgNS plasmon band, and the limited overlap of the ruthenium emission with this plasmon band, the measured 1.6-fold luminescence enhancement could imply an increase in the excitation rate rather than a modification of the RDR. The observed value of the lifetime ratio, however, suggested that the latter did in fact take place, because a decrease in lifetime occurred simultaneously with an improvement of the ruthenium quantum yield, which was estimated using (6) to be $Q_{\text{Metal}} \sim 0.40$ (see Table 1). The reason for this RDR increase could lie in the possibility that the nanoassembly may contain aggregates and/or dimers of silver nanospheres, whose plasmon modes are coupled and shifted to longer wavelengths. A red-shifted aggregate-AgNS plasmon band could slightly overlap with the ruthenium emission band, leading to the observed drop in the lifetime ratio and thus to a modest modification of ruthenium RDR.

It has to be emphasized that each of the four ruthenium-functionalized layers coupled differently to the surface plasmons of the nanospheres; thus, there is a range of actual Ru-to-metal distances for this configuration (the actual distances are larger than the spacer-layer thickness d used to characterize an assembly). Consequently, the observed enhancement factors and lifetime ratios are average values over various Ru-Np distances in the four functionalized layers.

Similar trends were observed when silver nanorods with an aspect ratio of ~12 (AgNR12) were used in the sensor region (see Table 1). Maximum enhancement of $\eta \sim 9.2$ occurred when the spacer-layer thickness was 8 nm (plot not shown here); the corresponding lifetime ratio and estimated quantum yield were $\tilde{\tau} \sim 0.74$ and $Q_{\text{Metal}} \sim 0.27$, respectively. In this case, the AgNR12 plasmonic band at lower energy, that is, the plasmon mode due to electron oscillations in the direction of the NR long axis, had a better overlap with the ruthenium emission band than with that of the AgNSs (see Figure 4), which supported the interpretation that the observed luminescence enhancement should be due in part to an increased RDR. An additional contribution to the enhancement may have arisen from overlap of the ruthenium absorption band with the AgNR plasmon resonances at higher energy due to plasmon excitation along the NR short axis, which is expected to increase the excitation rate.

When using silver triangles (AgNT), an enhancement factor of $\eta \sim 17.7$ and a lifetime ratio $\tilde{\tau} \sim 0.43$ were achieved (see Figure 6 and Table 1) for $d \sim 10$ nm. Concomitantly, the estimated quantum yield of the ruthenium complex rose to $Q_{\text{Metal}} \sim 0.57$. For this system the increase in the luminescence intensity, the decrease in the lifetime, and the increase in the quantum yield are most likely caused by an improvement on the radiative-decay pathway of ruthenium because of the coupling of the RuBITC-excited state to the AgNT plasmon resonance modes at higher wavelengths. From Figures 3(b) and 4 we also expect an excitation enhancement to contribute to the total RDR modification. It is important to recall that the excitation wavelength of 465 nm is offset from maximum of the plasmon resonance peaks for most of the nanostructures studied here (except for the AgNR12 case). Therefore, the change in molecular

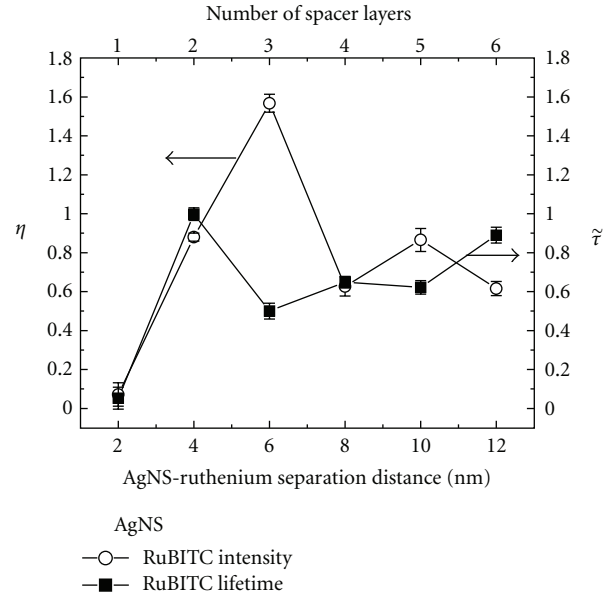

Figure 7: Enhancement factors η and lifetime ratios $\tilde{\tau}$ as function of the total spacer-layer thickness d (bottom axis) and number n of polyelectrolyte (double) layers (top axis) for the fibercore~AgNS-$(\text{PAH-PSS})_n$-(PAH~RuBITC) nanocomposite.

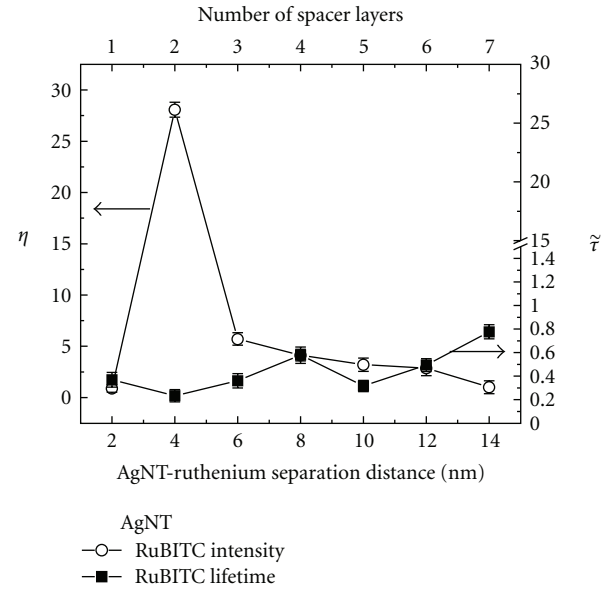

Figure 8: Enhancement factors η and lifetime ratios $\tilde{\tau}$ as function of the total spacer-layer thickness d (bottom axis) and number n of polyelectrolyte (double) layers (top axis) for the fibercore~AgNT-$(\text{PAH-PSS})_n$-(PAH~RuBITC) nanocomposite.

absorption mediated by the electric near field because of the plasmon of the nanoparticles is weak. This could explain why four ruthenium layers were needed to obtain a signal.

Our results are consistent with those obtained by Pan et al. [24], who showed that both excitation and emission effects contribute to the average luminescence enhancement observed with random colloidal films. This hypothesis is

Table 1: Enhancement factors η and luminescence lifetime ratios $\tilde{\tau}$ for RuBITC in crossed-optical-fiber sensor assemblies containing silver nanoparticles of different shapes. For each assembly, the spacer layer thickness d, which is the total distance from the nanoparticle surface to the first RuBITC-functionalized polyelectrolyte layer, excluding the functionalized layer, is given. The values Q_{Metal} are the estimated luminescence quantum yields in the presence of nanoparticles.

Np Shape	Four Layers PAH∼RuBITC-PSS				Single Layer PAH∼RuBITC-PSS			
	η	$\tilde{\tau}$	d (nm)	Q_{Metal}	η	$\tilde{\tau}$	d (nm)	Q_{Metal}
AgNS	1.63 ± 0.04	0.60 ± 0.06	8	0.40	1.55 ± 0.05	0.50 ± 0.04	6	0.50
AgNT	17.7 ± 0.3	0.43 ± 0.04	10	0.57	27.1 ± 0.7	0.23 ± 0.05	4	0.77
AgNR3	N/A	N/A	N/A	N/A	6.21 ± 0.02	0.40 ± 0.03	4	0.60
AgNR12	9.21 ± 0.06	0.74 ± 0.05	8	0.27	11.05 ± 0.04	0.54 ± 0.03	6	0.46

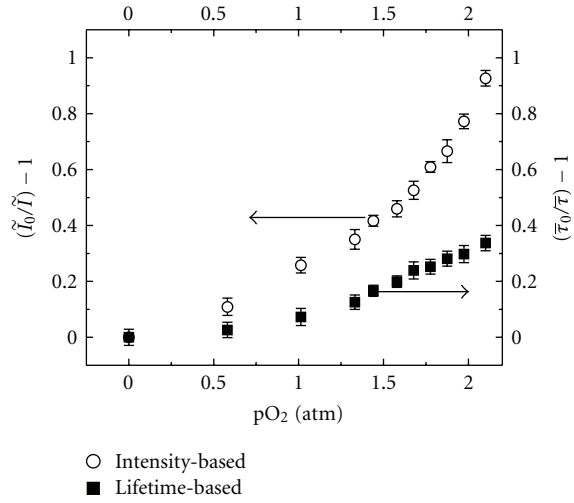

Figure 9: Calibration curves for intensity and lifetime observation of the response of the nanoengineered ruthenium sensor dyes to oxygen. $\tilde{I}_0$ ($\bar{\tau}_0$) and $\tilde{I}$ ($\bar{\tau}$) are the respective luminescence intensity (lifetime) in the absence and in the presence of oxygen. pO_2 is the oxygen partial pressure in the flow cell.

also reminiscent of the surface-enhanced Raman scattering (SERS) studies by McFarland et al. [25], who observed maximum SERS enhancement when both incident and Raman scattering photons experience local electromagnetic field enhancements. We believe that variations in RuBITC attachment orientation, and fiber-core coverage of AgNps as well nanoparticle shape inhomogeneity also play important roles in the coupling excited state of RuBITC to the nanoparticle plasmon resonance band.

3.3. LSP-Wavelength-Dependence of the Luminescence Enhancement. Next, we focused on the wavelength dependence of local-field enhancements around metal nanostructures. Instead of using as excitation wavelength the one that matched the maximum absorbance of ruthenium, we used the wavelength of the maximum of LSPR absorption band to excite the plasmons of the nanostructures. We found that using the optimum LSPR wavelength for a particular nanoparticle we could detect the emission of a single layer of ruthenium, irrespective of the AgNp shape. As described above, when using the optimum excitation wavelength of 465 nm for ruthenium, at least three extra functional layers were required to obtain a measurable signal for all the Nps shapes. Also, it has to be mentioned that in our experiment setup, the excitation laser pulses are coupled into the optical fibers such that many modes are populated. Most of these modes have evanescent fields with penetration depths much larger than the thickness of the functional layer(s). Thus, the differences observed for the enhancement factors and lifetime ratios of one and four functional layers are not caused by changes of the evanescent-field intensity at the functional layers, but are dominated by the chosen excitation wavelengths.

When the second excitation region of the optical fiber was coated with AgNS-$(\text{PAH-PSS})_n$-(PAH∼RuBITC-PSS) and an excitation wavelength of 410 nm was used (which corresponds to the highest AgNS plasmon absorption wavelength as seen in Figure 4) we observed values of $\eta \sim 1.6$ and $\tilde{\tau} \sim 0.50$ (see Figure 7), the latter value corresponding to an estimated quantum yield of $Q_{\text{Metal}} \sim 0.50$.

These values are similar to those obtained using four ruthenium layers and an excitation wavelength of 465 nm (see Table 1). However, the maximum enhancement was observed for $d \sim 6$ nm. Even though the values of η, $\tilde{\tau}$, and Q_{Metal} changed little, we obtained these using only one ruthenium layer, suggesting that at 410-nm excitation the generated AgNS-electromagnetic field is larger than the one generated with 465-nm excitation (off AgNs resonance). The observed drop in the lifetime ratio and the increase of the quantum yield from ∼0.40 to ∼0.50 compared to 465-nm excitation for this spacer-layer thickness suggested a larger modification of the RDR of ruthenium. Moreover, as explained above, AgNS agglomeration could have shifted the LSP band to longer wavelengths. An increase in the excitation rate is most likely to be the dominant enhancement effect in this case. As before, when ruthenium is very close to the AgNS surface, the luminescence intensity and lifetime are quenched.

Using silver nanorods with different aspect ratios (A/R), we could clearly observe the resonance-wavelength dependence of the AgNp plasmons. As a result of using AgNR with A/R ∼ 3 (AgNR3) values of $\eta \sim 6.2$, $\tilde{\tau} \sim 0.40$, and $Q_{\text{Metal}} \sim 0.60$ were found when RuBITC molecules for

a spacer-layer thickness of $d \sim 4$ nm (not shown here). The excitation wavelength was set to 410 nm (as for the AgNS configuration). When using AgNRs with A/R ~ 12 (AgNR12), the excitation wavelength was chosen to be 450 nm (see Figure 4). The values of $\eta \sim 11.1$, $\widetilde{\tau} \sim 0.55$, and $Q_{\text{Metal}} \sim 0.46$ was measured for $d \sim 6$ nm. Comparing the results obtained for AgNRs with different aspect ratios showed that similar values of $\widetilde{\tau}$ and Q_{Metal} were obtained (especially when compared to the quantum yield of ruthenium $Q_{\text{NonMetal}} \sim 0.008$ without interaction with nanoparticles). For both aspect ratios, the longitudinal AgNR plasmon absorption band overlapped poorly with the RuBITC emission band, with the AgNR3 longitudinal band maximum being at shorter wavelengths and the AgNR12 longitudinal plasmon band maximum being at longer wavelengths with respect to the maximum emission of ruthenium. Thus, only small differences in the RDR modification were expected. However, the magnitude of the RDR modification in both cases was substantial, particularly for AgNR3 with an estimated quantum yield of $Q_{\text{Metal}} \sim 0.60$! The larger difference found for the intensity enhancement factors, η, was caused mainly by different enhancements of the excitation rates, with the larger spectral overlap of the higher energy AgNR12 plasmon peak and ruthenium absorption band leading to larger values of η.

The highest intensity-enhancement factor for ruthenium was found using silver nanotriangles (AgNT). For a thickness of 4 nm of the spacer layer separating AgNT and the RuBITC-doped layer, values of $\eta \sim 27$, $\widetilde{\tau} \sim 0.23$, and $Q_{\text{Metal}} \sim 0.77$ were measured (see Figure 8), using an excitation wavelength of 440 nm. These results were a consequence of a more effective coupling of the AgNT dipole plasmon mode to the excited state of RuBITC, because of strong spectral correlation. As with AgNS's and AgNR's, for an excitation wavelength out of resonance with the plasmon band (close to the maximum of the dye absorption at 465 nm), three additional Ru-functionalized layers were needed to obtain measurable signals from the assembly; even though the number of RuBITC sensor molecules in the assembly was larger, the values determined for η and $\widetilde{\tau}$ (Table 1) were not as pronounced as those for the assembly with one-dye layer and excitation at 440 nm (Figure 8). Because the near-field enhancement is strongly distance dependent, the highest excitation rate should occur for luminophores directly adsorbed on nanoparticles, which exhibit an LSPR peak that directly overlaps with the maximum in the absorption spectrum of the ruthenium molecules. However, the luminescence quantum yield is also strongly distance dependent: for luminophores directly adsorbed on metal nanoparticles it is negligible because the coupling to the metal opens up new nonradiative decay pathways via energy transfer from the excited luminophore to the metal surface plasmon modes. This quenching is still dominant when ruthenium was at short distances (0–2 nm) from the metal surface (Figure 8). With a spacer-layer thickness of ~4 nm, quenching is dramatically reduced, leading to an increase in the RDR of the luminophore and, thus, of its luminescence quantum yield to $Q_{\text{Metal}} \sim 0.77$, because of the metal-altered local photonic mode density and the enhancement of the emission field by the surface plasmon field.

3.4. Plasmonic Optical-Fiber Sensor for Oxygen Measurement. After establishing that assemblies containing ruthenium molecules separated from AgNTs by a spacer layer of thickness $d \sim 4$ nm provided the maximum enhancement of the sensor emission intensity (~27-fold) when using an excitation wavelength of 440 nm, calibration curves for oxygen sensing via ruthenium luminescence intensity (and lifetime) changes were measured using the experimental setup described in Figure 2. The sensing mechanism is based on the collisional quenching of ruthenium luminescence by oxygen, which is described by the Stern-Volmer equation [26]. Most often for oxygen sensing studies sensor molecules are embedded in a polymer matrix; however, in this particular case, we electrostatically attached RuBITC to the AgNT. The sensor layer is very thin (~2 nm), which for the majority of the sensor molecules allows for the direct interaction with oxygen (some RuBITC molecules maybe buried in the outermost polyelectrolyte chain). This configuration is more desirable than the polymer-based optical-fiber sensors because it can overcame the analyte diffusion and mass-transfer problems commonly associated with bulk matrices.

The ruthenium response to gaseous oxygen is displayed in the Stern-Volmer plot in Figure 9. Each point in these calibration curves is an average of at least three different experiments (each with a newly prepared sensor assembly). The curvature of the Stern-Volmer plots indicates nonlinear oxygen quenching. This can be attributed to the existence of multiple decay profiles and species with different quenching probabilities [27–29] because some RuBITC molecules can be wrapped in the long polyelectrolyte chain, while others may be located at the outermost surface.

The sensor, however, shows an overall reduced dynamic range as compared to several nonmetalized ruthenium oxygen sensors where ruthenium was embedded in a polymer matrix [30–33]. The low quenching efficiency is not surprising because ruthenium molecules exhibit reduced lifetimes in the presence of metallic nanostructures, which resulted in a reduced net collisional quenching efficiency. We tried to compare the sensor capability of the AgNT-$(\text{PAH-PSS})_2$-(PAH~RuBITC-PSS) sensor after dissolving the silver nanotriangles; however, the low ruthenium intensity observed after increase the oxygen partial pressure up to 0.22 atm prevented the detection and quantification of $\widetilde{I}$ and $\overline{\tau}$.

We also measured how the lifetime of ruthenium responded to oxygen pressure changes. A multiexponential decay fit with two components corresponded most accurately with the collected data (see Section 2.6). The origin of the multiple decays can again be attributed to inhomogeneities in the polyelectrolyte layer. Molecules with different positioning relative to the metal Np will display different decay profiles. The extracted lifetimes (using (2)–(4)) were plotted as a function of oxygen partial pressure in Figure 9 as a Stern-Volmer plot. As expected, the lifetimes were significantly shortened (the measured lifetime of

ruthenium was ~100 ns in a nitrogen saturated atmosphere) compared to that of the sensor molecule in a polymer matrix (~817 ns in absence of oxygen [30]). Regardless of the reduced lifetimes of the probes in the presence of the metallic Nps, we were able to see a satisfactory lifetime response to oxygen, although its sensitivity was inferior to that of the intensity-based measurement. Following the observations of Lakowicz and Weber [34], this can be attributed to the dominance of luminescence-lifetime distributions over distributions of the bimolecular quenching constants, whereas the behavior observed here would suggest the opposite. With the majority of sensor molecules located at the sensor surface and, thus, directly accessible to oxygen, broad distributions of the bimolecular quenching constants are unlikely. On the other hand, given the disordered nature of the polyelectrolyte and the strong attachement of the ruthenium complex to the polyelectrolyte, distributions of the luminescence lifetimes are more likely to arise. Thus, the explanation of the observed behavior has to lie in the MEL effect, which reduces the luminescence lifetimes and possibly also the lifetime distributions to the extent that existing narrow distributions of the bimolecular quenching constants might predominate.

The actual response is that time could not be accurately estimated because of instrumentation limitations; however, we estimate that the response time should be significantly less than 1 s (the response time observed from a polymer-based oxygen sensor [30]). Because of the thickness of the PAH~RuBITC-PSS layer (~2 nm), the response time should not be diffusion-limited, but based on the interaction time between oxygen and the ruthenium molecules.

4. Conclusions

We demonstrated that the phenomenon of MEL can be used for the development of an optical-fiber sensor for oxygen determination. We determined that when the layer containing ruthenium molecules is separated by a spacer layer of 4 nm from silver nanotriangles on the fiber core the highest luminescence enhancement was obtained. Despite the decreased response range, oxygen sensing via intensity and lifetime changes was possible with a metal-modified ruthenium radiative decay rate. This was an unexpected result because it was believed that the lifetimes of the molecules would be so drastically reduced by the metal nanoparticle that any change would be undetectable.

Not only was sensing possible using a metal-modified ruthenium sensor assembly, but also using the high emission intensity allowed for sensing employing only a "single" layer of sensor molecules. This is important because it eliminates the diffusion limitations often seen in polymer-based sensors. As a result, the optical-fiber sensor provided a rapid response with a response time based only on the interaction of the oxygen with the ruthenium molecules. Moreover, because the need for diffusion to sensor sites is eliminated, MEL sensor assemblies may be employed for monitoring large molecules, which because of their size would have very low diffusion rates through bulk matrices, and monitoring analytes whose chemistry would be incompatible with the matrix composition.

Finally, our results indicated that the MEL effect significantly improved the emission of a luminophore with a moderate quantum yield. This means that luminophores that hitherto were rejected for sensing because of low quantum yields may now be revisited for sensing in combination with metal-enhancement effects.

Acknowledgments

This paper is based upon work supported in part by the National Science Foundation under Grant no. CHE-0723002 (MRI). Additional financial support by the University of Wisconsin-Milwaukee Research Growth Initiative is acknowledged. M. V. Rigo is grateful for the University of Wisconsin-Milwaukee Dissertation Fellowship and Dr. and Mrs. George Sosnovsky Award for Graduate Research. The authors would like to acknowledge Megan M. Schultz for measuring the luminescence quantum yield of the ruthenium complex in solution.

References

[1] F. Tam, C. Moran, and N. Halas, "Geometrical parameters controlling sensitivity of nanoshell plasmon resonances to changes in dielectric environment," *Journal of Physical Chemistry B*, vol. 108, no. 45, pp. 17290–17294, 2004.

[2] J. J. Mock, M. Barbic, D. R. Smith, D. A. Schultz, and S. Schultz, "Shape effects in plasmon resonance of individual colloidal silver nanoparticles," *The Journal of Chemical Physics*, vol. 116, no. 15, pp. 6755–6759, 2002.

[3] P. Royer, J. L. Bijeon, J. P. Goudonnet, T. Inagaki, and E. T. Arakawa, "Optical absorbance of silver oblate particles. Substrate and shape effects," *Surface Science*, vol. 217, no. 1-2, pp. 384–402, 1989.

[4] O. Stranik, R. Nooney, C. McDonagh, and B. D. MacCraith, "Optimization of nanoparticle size for plasmonic enhancement of fluorescence," *Plasmonics*, vol. 2, no. 1, pp. 15–22, 2007.

[5] J. Seo, W. -J. Kim, C. S. Ah et al., "Colorimetric analysis on flocculation of bioinspired Au self-assembly for biophotonic application," *Journal of Nanomaterials*, vol. 2009, Article ID 261261, 6 pages, 2009.

[6] O. Stranik, H. M. McEvoy, C. McDonagh, and B. D. MacCraith, "Plasmonic enhancement of fluorescence for sensor applications," *Sensors and Actuators B*, vol. 107, no. 1, pp. 148–153, 2005.

[7] J. R. Lakowicz, B. Shen, Z. Gryczynski, S. D'Auria, and I. Gryczynski, "Intrinsic fluorescence from DNA can be enhanced by metallic particles," *Biochemical and Biophysical Research Communications*, vol. 286, no. 5, pp. 875–879, 2001.

[8] J. R. Lakowicz, Y. Shen, S. D'Auria et al., "Radiative decay engineering: 2. Effects of silver island films on fluorescence intensity, lifetimes, and resonance energy transfer," *Analytical Biochemistry*, vol. 301, no. 2, pp. 261–277, 2002.

[9] P. Anger, P. Bharadwaj, and L. Novotny, "Enhancement and quenching of single-molecule fluorescence," *Physical Review Letters*, vol. 96, no. 11, Article ID 113002, 4 pages, 2006.

[10] J. N. Farahani, D. W. Pohl, H. J. Eisler, and B. Hecht, "Single quantum dot coupled to a scanning optical antenna: a tunable superemitter," *Physical Review Letters*, vol. 95, no. 1, Article ID 017402, 4 pages, 2005.

[11] S. Kühn, U. Håkanson, L. Rogobete, and V. Sandoghdar, "Enhancement of single-molecule fluorescence using a gold nanoparticle as an optical nanoantenna," *Physical Review Letters*, vol. 97, no. 1, Article ID 017402, 2006.

[12] E. Hao and G. C. Schatz, "Electromagnetic fields around silver nanoparticles and dimers," *The Journal of Chemical Physics*, vol. 120, no. 1, pp. 357–366, 2004.

[13] B. J. Prince, A. W. Schwabacher, and P. Geissinger, "A readout scheme providing high spatial resolution for distributed fluorescent sensors on optical fibers," *Analytical Chemistry*, vol. 73, no. 5, pp. 1007–1015, 2001.

[14] P. Geissinger and A. W. Schwabacher, "Applications of distributed optical fiber sensing: fluorescent assays of linear combinatorial arrays," in *Annual Review of Fluorescence*, C. D. Geddes and J. R. Lakowicz, Eds., vol. 1, pp. 164–194, Kluwer Academic/Plenum Publishers, New York, NY, USA, 2004.

[15] P. E. Henning, A. Benko, A. W. Schwabacher, P. Geissinger, and R. J. Olsson, "Apparatus and methods for optical time-of-flight discrimination in combinatorial library analysis," *Review of Scientific Instruments*, vol. 76, no. 6, Article ID 062220, 8 pages, 2005.

[16] A. Sileikaite, I. Prosycevas, J. Puiso, A. Juraitis, and A. Guobiene, "Analysis of silver nanoparticles produced by chemical reduction of silver salt solution," *Material Science*, vol. 12, no. 4, pp. 287–291, 2006.

[17] N. R. Jana, L. Gearheart, and C. J. Murphy, "Wet chemical synthesis of silver nanorods and nanowires of controllable aspect ratio," *Chemical Communications*, no. 7, pp. 617–618, 2001.

[18] T. C. Deivaraj, N. L. Lala, and J. Y. Lee, "Solvent-induced shape evolution of PVP protected spherical silver nanoparticles into triangular nanoplates and nanorods," *Journal of Colloid and Interface Science*, vol. 289, no. 2, pp. 402–409, 2005.

[19] G. Schneider and G. Decher, "Functional core/shell nanoparticles via layer-by-layer assembly. Investigation of the experimental parameters for controlling particle aggregation and for enhancing dispersion stability," *Langmuir*, vol. 24, no. 5, pp. 1778–1789, 2008.

[20] G. Schneider and G. Decher, "From functional core/shell nanoparticles prepared via layer-by-layer deposition to empty nanospheres," *Nano Letters*, vol. 4, no. 10, pp. 1833–1839, 2004.

[21] W. Xu, R. C. McDonough, B. Langsdorf, J. N. Demas, and B. A. DeGraff, "Oxygen sensors based on luminescence quenching: interactions of metal complexes with the polymer supports," *Analytical Chemistry*, vol. 66, no. 23, pp. 4133–4141, 1994.

[22] C. F. Bohren and D. R. Huffman, *Absorption and Scattering of Light by Small Particles*, Wiley Science, New York, NY, USA, 1993.

[23] A. T. R. Williams, S. A. Winfield, and J. N. Miller, "Relative fluorescence quantum yields using a Computer-controlled luminescence spectrometer," *The Analyst*, vol. 108, no. 1290, pp. 1067–1071, 1983.

[24] S. Pan, Z. Wang, and L. J. Rothberg, "Enhancement of adsorbed dye monolayer fluorescence by a silver nanoparticle overlayer," *Journal of Physical Chemistry B*, vol. 110, no. 35, pp. 17383–17387, 2006.

[25] A. D. McFarland, M. A. Young, J. A. Dieringer, and R. P. Van Duyne, "Wavelength-scanned surface-enhanced Raman excitation spectroscopy," *Journal of Physical Chemistry B*, vol. 109, no. 22, pp. 11279–11285, 2005.

[26] J. R. Lakowicz, *Principles of Fluorescence Spectroscopy*, Springer, York, NY, USA, 3rd edition, 2006.

[27] S. Draxler, M. E. Lippitsch, I. Klimant, H. Kraus, and O. S. Wolfbeis, "Effects of polymer matrices on the time-resolved luminescence of a ruthenium complex quenched by oxygen," *Journal of Physical Chemistry*, vol. 99, no. 10, pp. 3162–3167, 1995.

[28] J. N. Demas, B. A. Degraff, and W. Xu, "Modeling of luminescence quenching-based sensors: comparison of multisite and nonlinear gas solubility models," *Analytical Chemistry*, vol. 67, no. 8, pp. 1377–1380, 1995.

[29] S. J. Payne, G. L. Fiore, C. L. Fraser, and J. N. Demas, "Luminescence oxygen sensor based on a ruthenium(II) star polymer complex," *Analytical Chemistry*, vol. 82, no. 3, pp. 917–921, 2010.

[30] M. V. Rigo, R. Olsson, and P. Geissinger, "Crossed-optical-fiber oxygen sensors with intensity and temperature referencing for use in high-spatial-resolution sensor arrays," *Sensors & Transducers Journal*, vol. 113, no. 2, pp. 18–32, 2010.

[31] B. D. MacCraith, C. M. McDonagh, G. O'Keeffe et al., "Fibre optic oxygen sensor based on fluorescence quenching of evanescent-wave excited ruthenium complexes in sol-gel derived porous coatings," *The Analyst*, vol. 4, no. 118, pp. 385–388, 1993.

[32] R. A. Potyrailo and G. M. Hieftje, "Oxygen detection by fluorescence quenching of tetraphenylporphyrin immobilized in the original cladding of an optical fiber," *Analytica Chimica Acta*, vol. 370, no. 1, pp. 1–8, 1998.

[33] C. McDonagh, B. D. MacCraith, and A. K. McEvoy, "Tailoring of sol-gel films for optical sensing of oxygen in gas and aqueous phase," *Analytical Chemistry*, vol. 70, no. 1, pp. 45–50, 1998.

[34] J. R. Lakowicz and G. Weber, "Quenching of protein fluorescence by oxygen. Detection of structural fluctuations in proteins on the nanosecond time scale," *Biochemistry*, vol. 12, no. 21, pp. 4171–4179, 1973.